Supporting Information (SI)

Four-membered red iridium(III) complexes with Ir-S-C-S structures for efficient organic light-emitting diodes

Ning Su,[a,b] Fang-Ling Li,[a] You-Xuan Zheng[a*]

a *State Key Laboratory of Coordination Chemistry, Jiangsu Key Laboratory of Advanced Organic Materials, School of Chemistry and Chemical Engineering, Nanjing University, Nanjing 210093, P. R. China.*

E-mail: yxzheng@nju.edu.cn

b College of Physics and Optoelectronic Engineering, Shenzhen University, Shenzhen 518060, China.

E-mail: suning@szu.edu.cn

Materials and Measurements.

All reagents and chemicals were purchased from commercial sources and used without further purification. ^{1}H NMR and ^{19}F NMR were measured on a Bruker AM 400 spectrometer. High-resolution electrospray mass spectra (HRMS) was measured on G6500 from Agilent for complexes. TGA measurements were carried out on a DSC 823e analyzer (METTLER). Absorption and photoluminescence spectra were measured on a UV-3100 spectrophotometer and a Hitachi F-4600 photoluminescence spectrophotometer, respectively. The decay lifetimes were measured with an Edinburgh Instruments FLS-980 fluorescence spectrometer in degassed CH_2Cl_2 solution at room temperature. The luminescence quantum efficiencies were calculated by comparison of the emission intensities (integrated areas) of a standard sample (*fac*-Ir(ppy)$_3$) and the unknown sample.

X-ray Crystallography.

The single crystals of complexes were carried out on a Bruker SMART CCD diffractometer using monochromated Mo Kα radiation (λ = 0.71073 Å) at room temperature. Cell parameters were retrieved using SMART software and refined using SAINT [1] on all observed reflections.

Data were collected using a narrow-frame method with scan widths of 0.30° in ω and an exposure time of 10 s/frame. The highly redundant data sets were reduced using SAINT and corrected for Lorentz and polarization effects. Absorption corrections were applied using SADABS [2] supplied by Bruker. The structures were solved by direct methods and refined by full-matrix least-squares on *F*2.[3] The positions of metal atoms and their first coordination spheres were located from direct-methods E-maps; other non-hydrogen atoms were found in alternating difference Fourier syntheses and least-squares refinement cycles and, during the final cycles, refined anisotropically. Hydrogen atoms were placed in calculated position and refined as riding atoms with a uniform value of Uiso.

Details of cyclic voltammetry measurements.

Cyclic voltammetry measurements were conducted on a MPI-A multifunctional electrochemical and chemiluminescent system (Xi'an Remex Analytical Instrument Ltd. Co., China) at room temperature, with a polished Pt plate as the working electrode, platinum thread as the counter electrode and Ag-$AgNO_3$ (0.1 M) in CH_2Cl_2 as the reference electrode, *tetra*-n-butylammonium perchlorate (0.1 M) was used as the supporting electrolyte, using Fc^+/Fc as the internal standard, the scan rate was 0.1 V s^{-1}.

OLEDs fabrication and measurement.

All OLEDs were fabricated on the pre-patterned ITO-coated glass substrate with a sheet resistance of 15 Ω sq^{-1}. The deposition rate for organic compounds is 1-2 Å s^{-1}. The phosphor and the host (TCTA/ 2,6DCzPPy) was co-evaporated to form emitting layer from two separate sources. The cathode consisting of LiF/ Al was deposited by evaporation of LiF with a deposition rate of 0.1 Å s^{-1} and then by evaporation of Al metal with a rate of 3 Å s^{-1}. The characteristic curves of the devices were measured with a computer which controlled KEITHLEY 2400 source meter with a calibrated silicon diode in air without device encapsulation. On the basis of the uncorrected PL and EL spectra, the Commission Internationale de l'Eclairage (CIE) coordinates were calculated using a test program of the Spectra scan PR650 spectrophotometer.

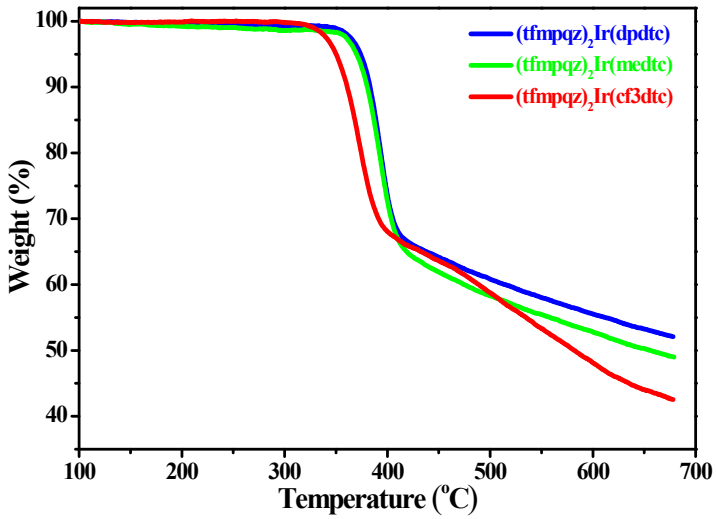

Fig. S1 TGA curves of $(tfmpqz)_2Ir(dpdtc)$, $(tfmpqz)_2Ir(medtc)$ and $(tfmpqz)_2Ir(cf3dtc)$ complexes.

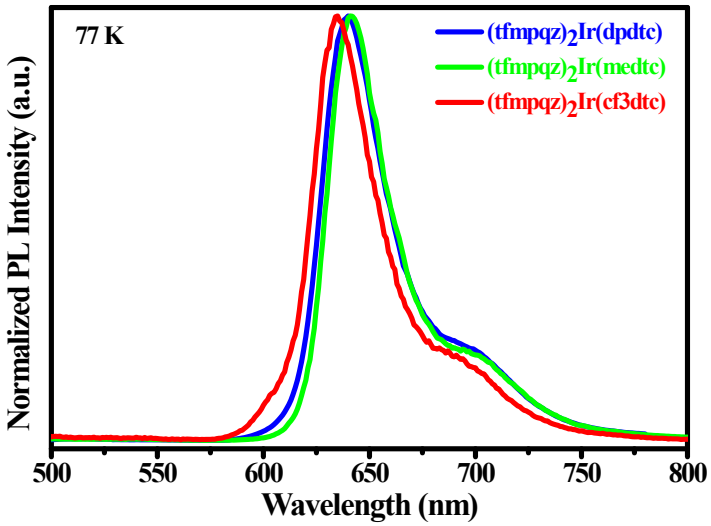

Fig. S2 The 77 K phosphorescent spectra of $(tfmpqz)_2Ir(dpdtc)$, $(tfmpqz)_2Ir(medtc)$ and $(tfmpqz)_2Ir(cf3dtc)$ complexes.

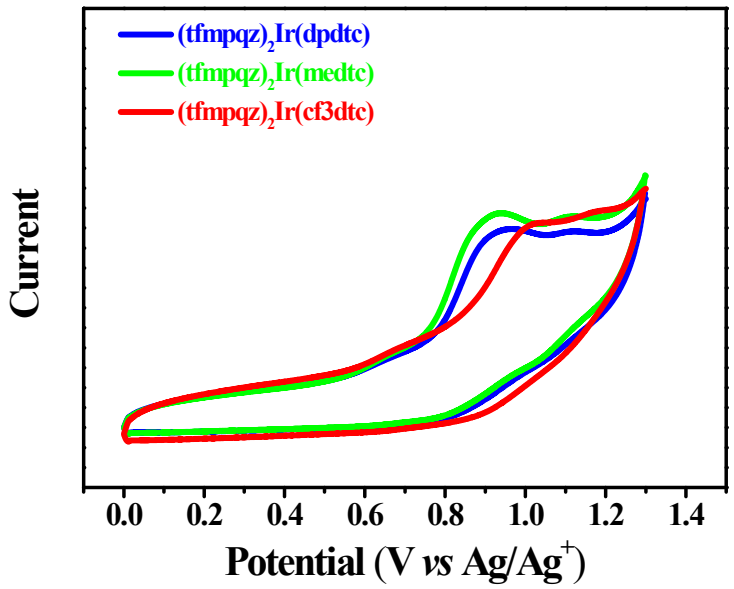

Fig. S3 CV curves of $(tfmpqz)_2Ir(dpdtc)$, $(tfmpqz)_2Ir(medtc)$ and $(tfmpqz)_2Ir(cf3dtc)$ complexes.

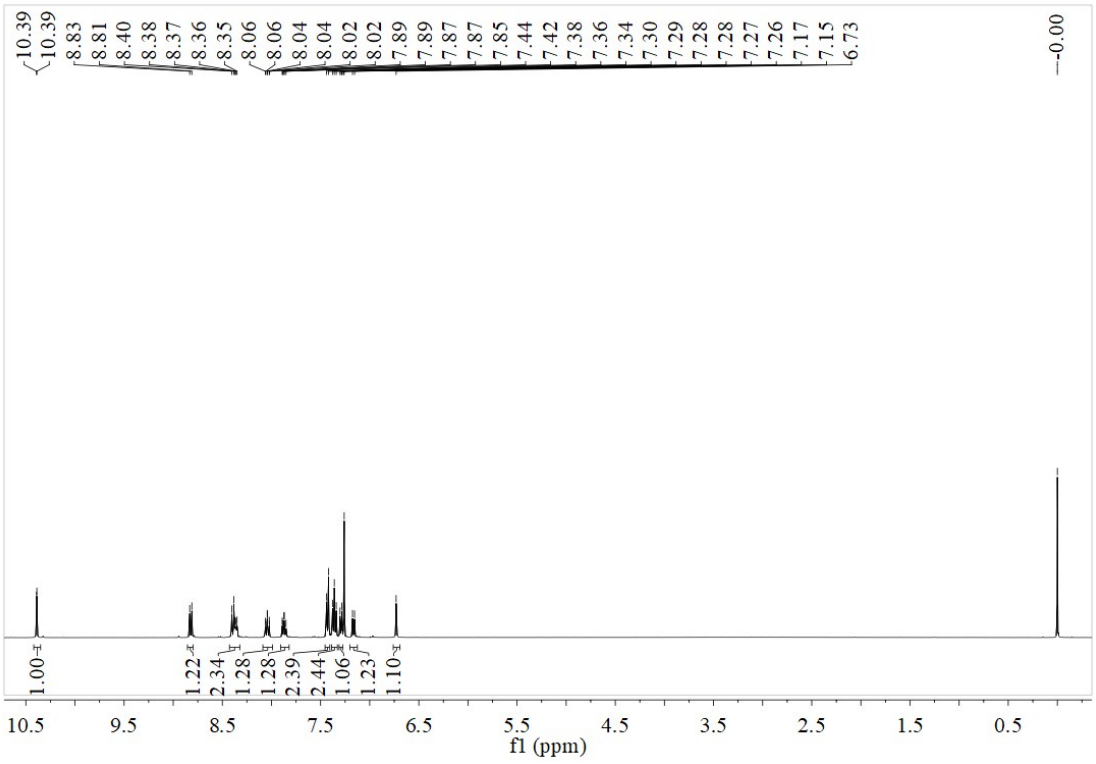

Fig. S4 ^1H NMR spectrum of $(tfmpqz)_2Ir(dpdtc)$ complex.

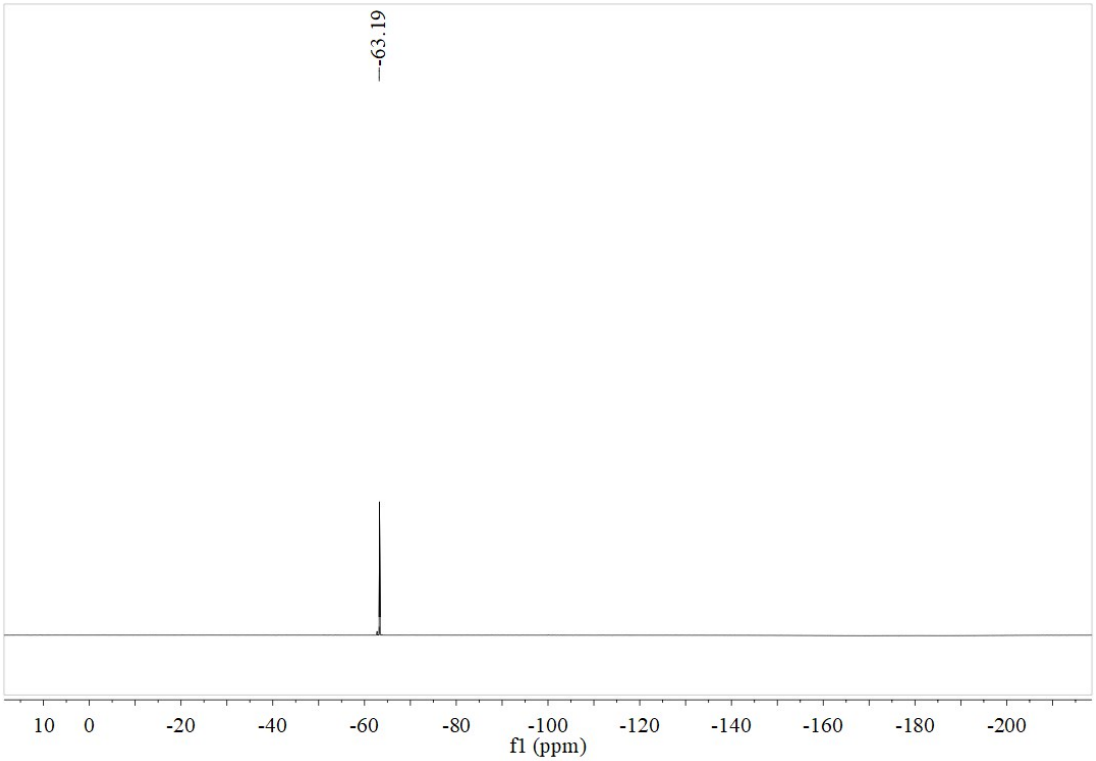

Fig. S5 ^{19}F NMR spectrum of $(tfmpqz)_2Ir(dpdtc)$ complex.

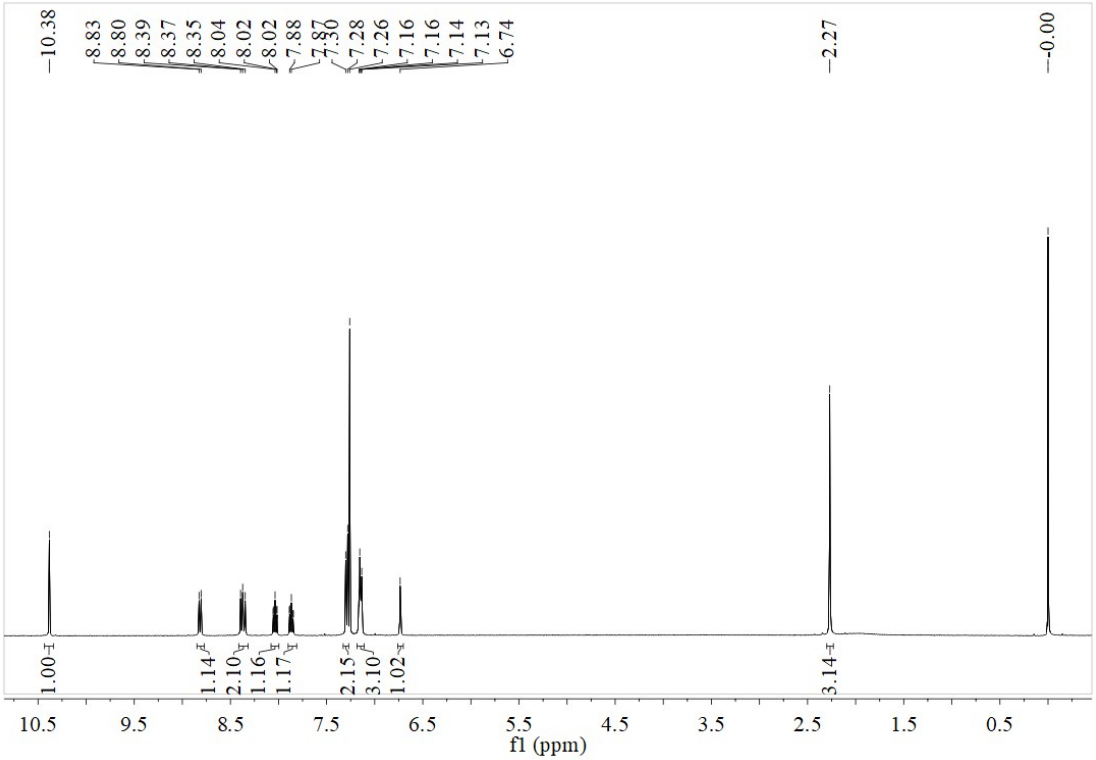

Fig. S6 ^{1}H NMR spectrum of $(tfmpqz)_2Ir(medtc)$ complex.

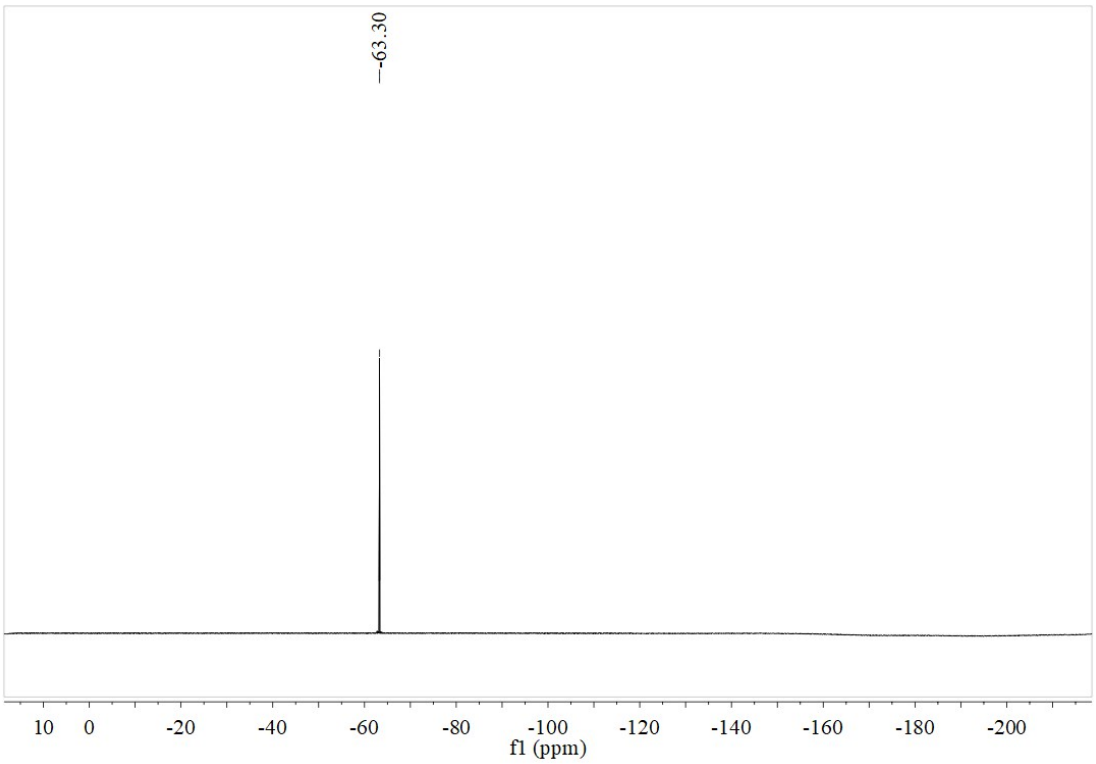

Fig. S7 ^{19}F NMR spectrum of $(tfmpqz)_2Ir(medtc)$ complex.

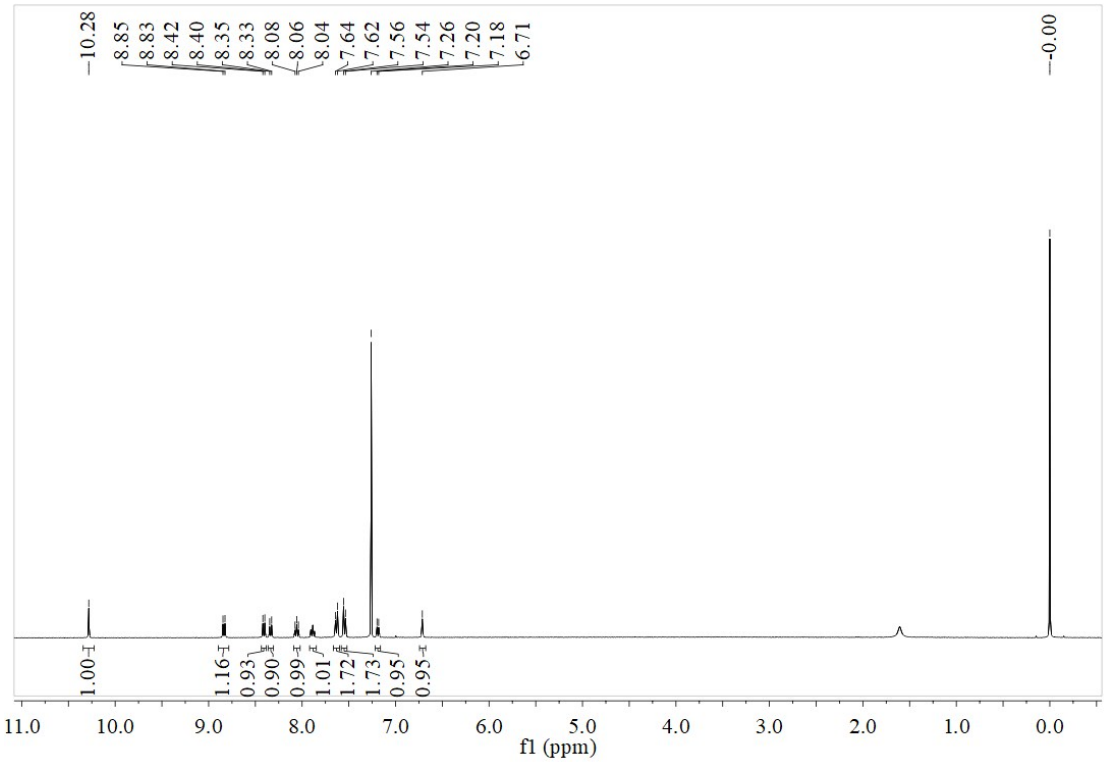

Fig. S8 ^{1}H NMR spectrum of $(tfmpqz)_2Ir(cf3dtc)$ complex.

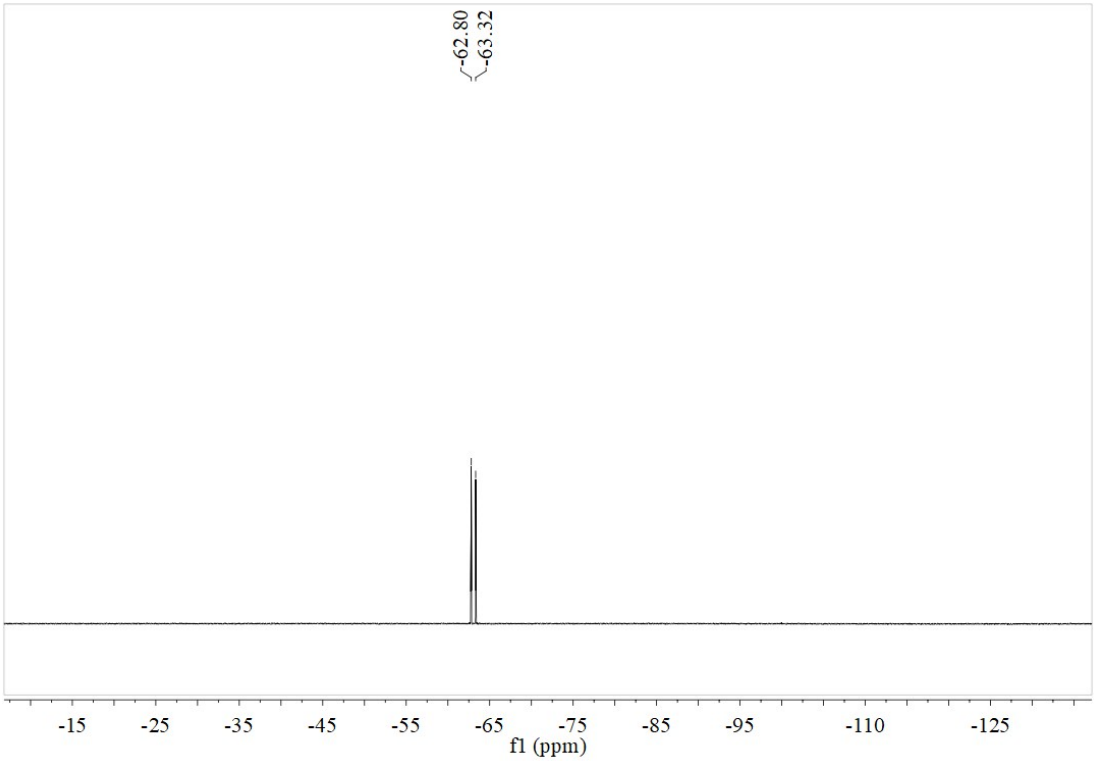

Fig. S9 ^{19}F NMR spectrum of $(tfmpqz)_2Ir(cf3dtc)$ complex.

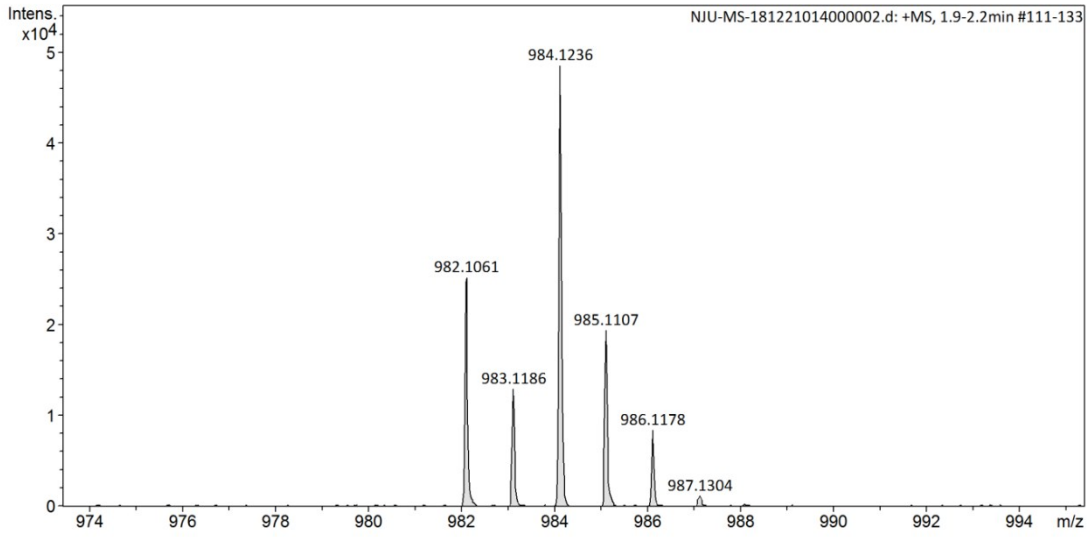

Fig. S10 HRMS spectrum of $(tfmpqz)_2Ir(dpdtc)$ complex.

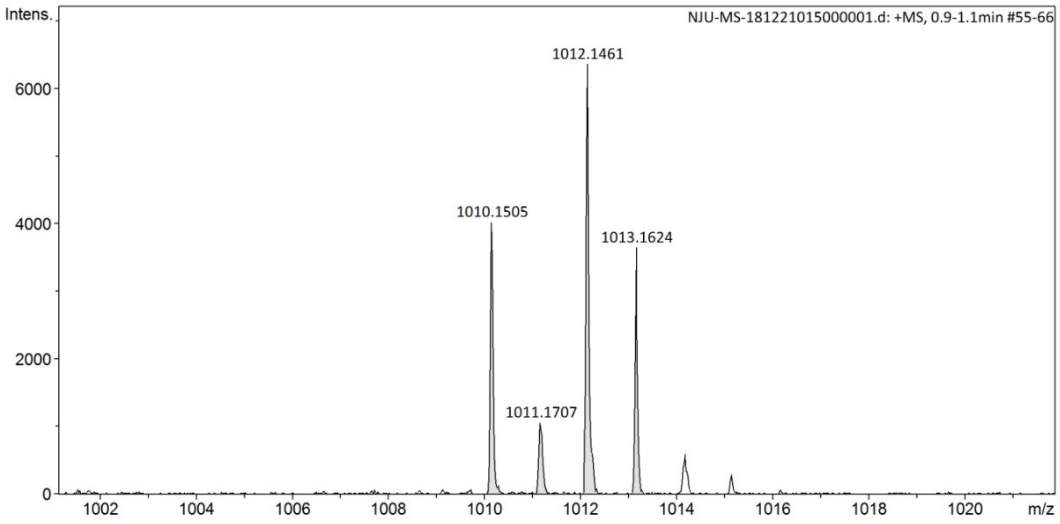

Fig. S11 HRMS spectrum of $(tfmpqz)_2Ir(medtc)$ complex.

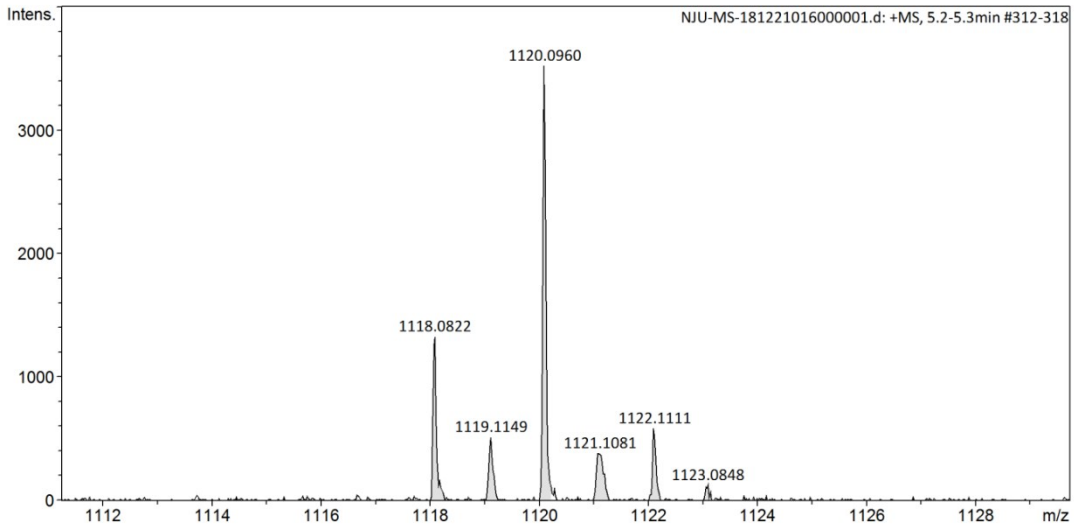

Fig. S12 HRMS spectrum of $(tfmpqz)_2Ir(cf3dtc)$ complex.

Table S1. Crystal information of $(tfmpqz)_2Ir(dpdtc)$, $(tfmpqz)_2Ir(medtc)$ and $(tfmpqz)_2Ir(cf3dtc)$ complexes.

	$(tfmpqz)_2Ir(dpdtc)$	$(tfmpqz)_2Ir(medtc)$	$(tfmpqz)_2Ir(cf3dtc)$
Formula	$C_{43}H_{26}F_6IrN_5S_2$	$C_{45}H_{30}F_6IrN_5S_2$	$C_{45}H_{24}F_{12}IrN_5S_2$
Formula weight	983.01	1011.06	1119.01
T (K)	173 (2)	173 (2)	296 (2)
Wavelength (Å)	0.71073	0.71073	0.71073
Crystal system	Monoclinic	Monoclinic	Monoclinic
Space group	$P2_1/n$	$C2/c$	$P2_1/c$
a (Å)	12.3627 (6)	10.442 (11)	10.4204 (6)
b (Å)	16.1241 (7)	23.68 (3)	26.2335 (16)

c (Å)	19.8219 (8)	15.834 (16)	16.5370 (10)
α (deg)	90.00	90.00	90.00
β (deg)	103.0820 (10)	106.52 (2)	107.1480 (10)
γ (deg)	90.00	90.00	90.00
V (Å^3)	3848.7 (3)	3754 (7)	4319.7 (4)
Z	4	4	4
ρ_{calcd} (g/cm^3)	1.696	1.789	1.721
μ (Mo Kα) (mm^{-1})	3.646	3.741	3.279
F (000)	1928	1992	2184
Range of transm factors	2.111 - 25.009	2.264 - 25.010	1.054 - 25.009
Reflns collected	27640	4585	24278
Unique(R_{int})	6786 (0.0428)	3294 (0.0350)	7619 (0.0453)
$R_1{}^a$, $wR_2{}^b$ [I > 2s(I)]	0.0255, 0.0517	0.0570, 0.1400	0.0406, 0.0816
$R_1{}^a$, $wR_2{}^b$ (all data)	0.0389, 0.0557	0.0693, 0.1497	0.0655, 0.0903
GOF on F^2	1.043	1.107	1.042
CCDC No.	1891565	1885951	1885886

$R_1{}^a = \Sigma||F_o| - |F_c||/\Sigma F_o|$. $wR_2{}^b = [\Sigma w(F_o{}^2 - F_c{}^2)^2/\Sigma w(F_o{}^2)]^{1/2}$

Table S2. Selected bond lengths and angles of $(tfmpqz)_2Ir(dpdtc)$, $(tfmpqz)_2Ir(medtc)$ and $(tfmpqz)_2Ir(cf3dtc)$ complexes.

$(tfmpqz)_2Ir(dpdtc)$		$(tfmpqz)_2Ir(medtc)$		$(tfmpqz)_2Ir(cf3dtc)$	
Selected bonds					
C20-Ir1	2.002 (4)	C1-Ir1	1.955 (8)	Ir1-C45	2.003 (6)
C43-Ir1	2.005 (3)	N1-Ir1	2.005 (7)	Ir1-C44	2.016 (5)
Ir1-N2	2.033 (3)	N1^i-Ir1	2.004 (7)	Ir1-N2	2.031 (5)
Ir1-N3	2.032 (3)	Ir1-S1	2.412 (3)	Ir1-N5	2.057 (4)
Ir1-S1	2.468 (8)	Ir1-S1^i	2.412 (3)	Ir1-S1	2.4503 (16)
Ir1-S2	2.470 (9)	S1-C16	1.669 (7)	Ir1-S2	2.4801 (18)
C36-S1	1.703 (4)	S1^i-C16	1.669 (7)	C28-N7	1.359 (8)
C36-S2	1.719 (3)	C16-N3	1.312 (16)	C28-S1	1.705 (6)
C36-N5	1.342 (4)	C1-Ir1-N1	77.5 (3)	C28-S2	1.701 (6)
Selected angles					
C20-Ir1-N3	78.95 (14)	S1-Ir1-S1^i	71.14 (13)	C44-Ir1-N2	78.7 (2)
C43-Ir1-N2	78.30 (12)	S1-C16-S1^i	114.4 (7)	C45-Ir1-N5	79.3 (2)

S1-Ir1-S2	71.50 (3)	C1-Ir1-C1^{i}	94.5 (5)	S1-Ir1-S2	71.60 (6)

Table S3. HOMO and LUMO electron cloud density distributions of each fragment of three Ir(III) complexes.

Complex	Orbit	Composition(%)		
		tfmpqz	Ir atom	ancillary ligand
$(tfmpqz)_2Ir(dpdtc)$	HOMO	43.55	47.66	8.79
	LUMO	93.51	4.08	2.41
$(tfmpqz)_2Ir(medtc)$	HOMO	41.80	48.78	9.43
	LUMO	94.29	3.53	2.17
$(tfmpqz)_2Ir(cf3dtc)$	HOMO	40.77	48.54	10.69
	LUMO	91.33	3.60	5.06